

# Boosting Discriminative Visual Representation Learning with Scenario-Agnostic Mixup

Siyuan Li\* Zicheng Liu\* Di Wu Zihan Liu Stan Z. Li  
AI Lab, School of Engineering, Westlake University, Hangzhou, Zhejiang, China

## Abstract

Mixup is a popular data-dependent augmentation technique for deep neural networks, which contains two sub-tasks, mixup generation and classification. The community typically confines mixup to supervised learning (SL) and the objective of generation sub-task is fixed to the sampled pairs instead of considering the whole data manifold. To overcome such limitations, we systematically study the objectives of two sub-tasks and propose **Scenario-Agnostic Mixup** for both SL and Self-supervised Learning (SSL) scenarios, named SAMix. Specifically, we hypothesize and verify the core objective of mixup generation as optimizing the local smoothness between two classes subject to global discrimination from other classes. Based on this discovery,  $\eta$ -balanced mixup loss is proposed for complementary training of the two sub-tasks. Meanwhile, the generation sub-task is parameterized as an optimizable module, *Mixer*, which utilizes an attention mechanism to generate mixed samples without label dependency. Extensive experiments on SL and SSL tasks demonstrate that SAMix consistently outperforms leading methods by a large margin.

## 1. Introduction

One of the fundamental problems in machine learning is to learn a proper low-dimensional representation efficiently that captures the intrinsic structures of data and facilitates downstream tasks [2, 5, 12, 27]. Data mixing, as a means of generating symmetric mixed data and labels, largely improves the quality of deep neural networks (DNNs) learning discriminative representation in various scenarios [11, 26, 30, 56]. Despite its general application, the policy of the generation process in data mixing requires an *explicit* design. For example, in computer vision, mixed samples are constructed by linear convex interpolation or random local patch replacement of sample pairs [54, 56]. In addition, classification labels can be used for generating task-relevant mixed samples to match labels such as offline

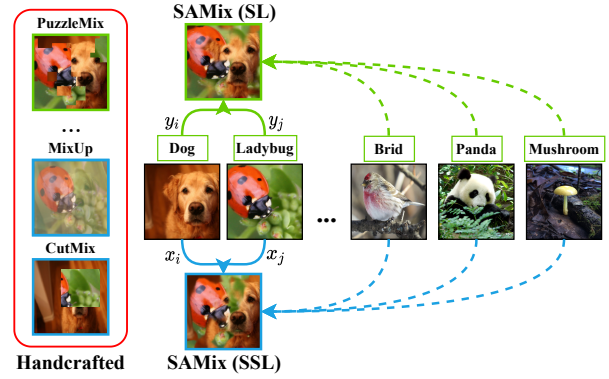


Figure 1. Mixed samples with green boxes rely on labels, while those with blue boxes do not. The solid line indicates that the local relationship directly influence to the mixed sample, and the dashed line indicates that the other class samples are a global constraint on the current mixed sample. Compared to handcrafted mixup policies that focus only on local sample pair, SAMix can generate semantic mixed samples by exploiting the local and global information and has no dependency on labels.

maximizing saliency information (e.g., gradCAM [40]) of related samples [25, 26, 46] and sample interpolation by adversarial training [57].

These handcrafted mixing policies as shown in the red box of Figure 1, however, fixed the objective of mixed data generation task in the data pairs (used to generate mixed data) and the label-dependent approaches are only limited in supervised learning (SL) scenarios, which may no be available in other scenarios such as self-supervise learning (SSL) [15, 17]. There are two remaining open problems: **how to design a learnable scenario-agnostic mixup policy and a proper mixup generation objective for preserving the task-relevant semantic correspondence**. Most current works tried to solve the simplified above questions, which directly transfers linear mixup methods into contrastive learning [23, 30, 41]. Although simple, these approaches do not exploit the underlying structure of the data manifold. In this paper, we propose SAMix (Figure 1), which stands for **Scenario-Agnostic Mixup**, an framework employs *Mixer* to generate mixed samples adaptively either at *instance-level* or *cluster-level*. To guarantee the task-

\*Equal contribution

relevant information can be captured by Mixer, we propose  *$\eta$ -balanced mixup loss* for treating mixup generation and classification differently from local and global perspective. Furthermore, for SSL scenarios, we propose a simple and effective *cross-view pipeline*, which significantly improves the performance of mixup methods without changing to original algorithms. Extensive experiments on both SL and SSL demonstrate the effectiveness and generalizability of SAMix. Our contributions are as follows:

- We design an learnable mixed sample generator, Mixer, adopting mixing attention and non-linear content modeling to capture task-relevant information.
- We summarize the mixup generation objective as optimizing the local smoothness subject to global discrimination and propose  $\eta$ -balanced mixup loss.
- We analyze the properties of mixup classification and propose an efficient cross-view pipeline for SSL.
- Combining the above, a scenario-agnostic mixup training framework is proposed for supervised and self-supervised learning and we conduct comprehensive experiments to prove the state-of-the-art performance.

## 2. Problem Definition

Given a finite set of i.i.d samples,  $X = [x_i]_{i=1}^n \in \mathbb{R}^{D \times n}$ , each data  $x_i \in \mathbb{R}^D$  is drawn from a mixture of, say  $C$ , distributions  $\mathcal{D} = \{\mathcal{D}_c\}_{c=1}^C$ . Our basic assumption for discriminative representations is that the each component distribution  $\mathcal{D}_c$  has relatively low-dimensional intrinsic structures, *i.e.*, the distribution  $\mathcal{D}_c$  is constrained on a sub-manifold, say  $\mathcal{M}_c$  with dimension  $d_c \ll D$ . The distribution  $\mathcal{D}$  of  $X$  is consisted of these sub-manifolds,  $\mathcal{M} = \cup_{c=1}^C \mathcal{M}_c$ . In a discriminative problem, we seek a low-dimensional representation  $z_i \in \mathcal{M}$  of  $x_i$  by learning a continuous mapping modeled by a network encoder,  $f_\theta(x) : x \mapsto z$  with the parameter  $\theta \in \Theta$ , which captures intrinsic structures of  $\mathcal{M}$  and facilitates the discriminative tasks.

### 2.1. Discriminative Representation Learning

**Parametric training with class supervision.** *Some supervised class information* is available to ease the discriminative tasks in practical scenarios, such as the class labels in supervised learning (SL) or the cluster number  $C$  in clustering (C). Here, we assume that a one-hot label  $y_i \in \mathbb{R}^C$  of each sample  $x_i$  can be somehow obtained,  $Y = [y_1, y_2, \dots, y_n] \in \mathbb{R}^{C \times n}$ . We denote the labels generated or adjusted during training as pseudo labels (PL), while the fixed as ground truth labels (L). Notice that each component  $\mathcal{D}_c$  is considered *separated* according to  $Y$  in this scenario. Then, a *parametric* classifier,  $g_\omega(z) : z \mapsto p$

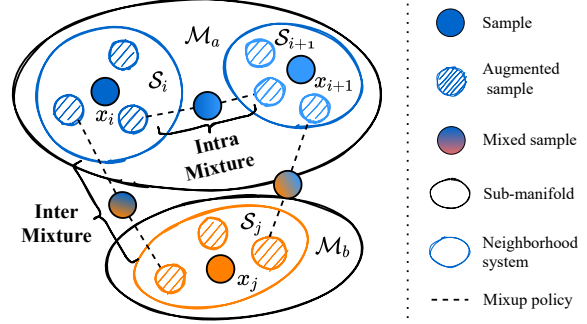


Figure 2. The class  $a$  and  $b$  are constrained on class sub-manifolds  $\mathcal{M}_a$  and  $\mathcal{M}_b$ , while a neighborhood system  $\mathcal{S}_i$  is defined by augmented views of  $x_i$ . We hope that inter-class mixed samples can prompt more discriminative representations.

with the parameter  $\omega \in \Omega$ , can be learned to map the representation  $z_i$  of each sample to its class label  $y_i$  by predicting the probability of  $p_i$  being assigned to the  $c$ -th class using the softmax criterion,  $p_{c|i} = \frac{\exp(w_c^T z_i)}{\sum_{j=1}^C \exp(w_j^T z_i)}$ , where  $w_c$  is a weight vector for the class  $c$ , and  $w_c^T z_i$  measures how similar between  $z_i$  and the class  $c$ . The learning objective is to minimize the cross-entropy loss (CE) between  $y_i$  and  $p_i$ ,

$$\ell^{CE}(y_i, p_i) = -y_i \log p_i. \quad (1)$$

As in information bottleneck (IB) [44], optimizing Eq. 1 is equal to maximizing the mutual information  $I(z, y)$  between  $z$  and  $y$  (as task-relevant information) while minimizing  $I(x, z)$  between  $x$  and  $z$  (as task-irrelevant information),  $\max_{\theta, \omega} I(z, y) - \beta I(x, z)$ , where  $\beta > 0$ .

**Non-parametric training as instance discrimination.** Complementary to the above parametric settings, *non-parametric* approaches are usually adopted in unsupervised scenarios (label-free). Due to the *lack of class information*, an instance discriminative task can be designed based on an assumption of local compactness: the low-dimensional neighborhood systems  $\mathcal{S}_i \in \mathbb{R}^{d_i}$  of  $x_i$  is invariant to a set of predefined augmentations  $\mathcal{T}$ , *i.e.*,  $x_i \in \mathcal{S}_i$  iff  $\tau(x_i) \in \mathcal{S}_i$  for all  $\tau \in \mathcal{T}$ . We mainly discuss contrastive learning (CL) and take MoCo [17] as an example. Consider a pair of augmented image  $(x_i^{\tau_q}, x_i^{\tau_k})$  from the same instance  $x_i \in \mathbb{R}^{C \times H \times W}$ , the local compactness is introduced by alignment of the encoded representation pair  $(z_i^{\tau_q}, z_i^{\tau_k})$  from  $f_{\theta, q}$  and the momentum  $f_{\theta, k}$ , and constrained to the global uniformity by contrasting  $z_i^{\tau_q}$  to a momentum dictionary of encoded keys from other images,  $\{z_j^{\tau_k}\}_{j=1}^K$ , where  $K$  denotes the length of the dictionary. It can be achieved by the popular non-parametric CL loss, called infoNCE [47]:

$$\ell^{NCE}(z_i^{\tau_q}, z_i^{\tau_k}) = -\log \frac{\exp(z_i^{\tau_q} z_i^{\tau_k} / t)}{\sum_{j=1}^K \exp(z_i^{\tau_q} z_j^{\tau_k} / t)}, \quad (2)$$

where  $t$  is a temperature hyper-parameter. Notice that a MLP projection neck,  $g_\omega(z) : z \mapsto p$ , is commonly adopted in

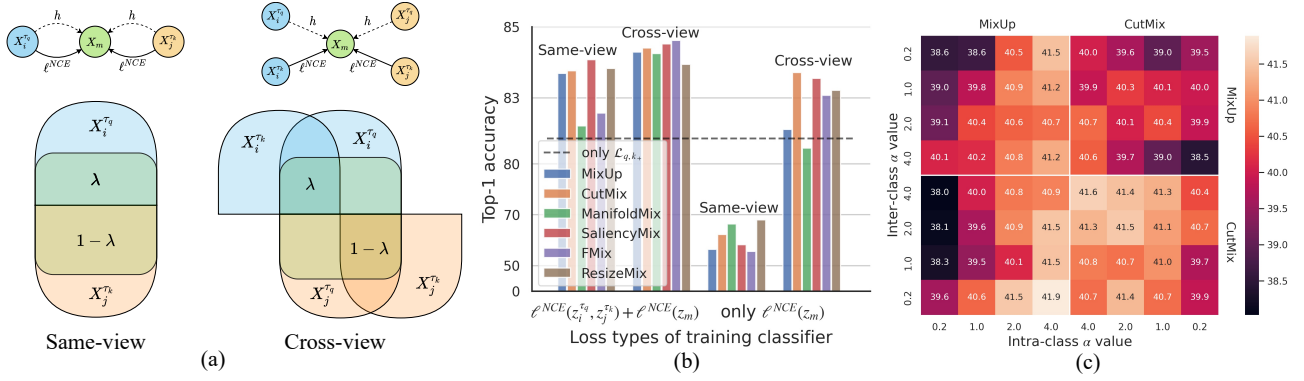


Figure 3. (a) Graphical models and information diagrams of *same-view* and *cross-view* training pipeline for instance-level mixup. Taking the *cross-view* as an example,  $x_m = h(x_i^{\tau_q}, x_j^{\tau_k}, \lambda)$ , the  $\lambda$  region denotes the corresponding information partition for  $\lambda I(z_m^{\tau_q}, z_i^{\tau_k})$  and the  $1 - \lambda$  region for  $(1 - \lambda)I(z_m^{\tau_q}, z_j^{\tau_k})$ . (b) Linear evaluation (Tiny top-1 accuracy) under whether to use the cross-view pipeline and to combine the original and mixup infoNCE loss. (c) A heat map of linear evaluation (Tiny top-1 accuracy) represents the effects of using MixUp and CutMix as the inter-class (y-axis) and intra-class mixup (x-axis) using various  $\alpha$ .

CL to calculate Eq. 2 since [5],  $\ell^{NCE}(p_i^{\tau_q}, p_i^{\tau_k})$ , where  $p = \frac{g(p)}{\|g(p)\|}$ . We still use the notation  $z$  as the SSL representation for simplicity. Comparing to Eq. 1, minimizing Eq. 2 equivalently maximizes a lower bound on  $I(z_i^{\tau_q}, z_i^{\tau_k})$  as discussed in [42, 47], i.e.,  $I(z_i^{\tau_q}, z_i^{\tau_k}) \geq \log(K) - \ell^{NCE}(z_i^{\tau_q}, z_i^{\tau_k})$ .

## 2.2. Mixup for Discriminative Representation

Recall two sub-tasks in mixup training: (a) *mixed data generation* and (b) *mixup classification*. As for the sub-task (a), two mixup functions are defined,  $h(\cdot)$  and  $v(\cdot)$ , to generate mixed samples and corresponding the mixed labels with a mixing ratio  $\lambda \sim \text{Beta}(\alpha, \alpha)$ . Given the mixed data, (b) defines a mixup training objective to optimize the inter-class discriminative relationships.

**Mixup classification as the main task.** We first define two types of the mixup classification objective  $\mathcal{L}_{\theta, \omega}$  for parametric and non-parametric training scenarios, *class-level* and *instance-level* mixup. As for parametric training, given two randomly selected data pairs,  $(x_i, y_i)$  and  $(x_j, y_j)$ , the mixed data is generated as  $x_m = h(x_i, x_j, \lambda)$  and  $y_m = v(y_i, y_j, \lambda)$ . The class-level mixup objective is:

$$\ell^{CE}(p_m) = \lambda \ell^{CE}(y_m, p_m) + (1 - \lambda) \ell^{CE}(y_m, p_m). \quad (3)$$

Notice that we fix  $v(\cdot)$  as the linear interpolation in our discussions, i.e.,  $v(y_i, y_j, \lambda) \triangleq \lambda y_i + (1 - \lambda) y_j$ . Symmetrically, we denote  $h(\cdot)$  as a pixel-wise mixing policy with element-wise product  $\odot$  for most input mixup methods [26, 54, 56], i.e.,  $x_m = s_i \odot x_i + s_j \odot x_j$ , where  $s_i \in \mathbb{R}^{H \times W}$  is a pixel-wise mask and  $s_j = 1 - s_i$ . Notice that each coordinate  $s_{w, h} \in [0, 1]$ . Similarly to Eq. 3, we can generate  $x_m$  with a pair of randomly selected samples  $(x_i, x_j)$  and formulate mixup infoNCE loss for instance-level mixup:

$$\ell^{NCE}(z_m) = \lambda \ell^{NCE}(z_m, z_i) + (1 - \lambda) \ell^{NCE}(z_m, z_j), \quad (4)$$

where  $z_m, z_i$  and  $z_j$  denote the representation of  $x_m$  and corresponding instances.

**Mixup generation as the auxiliary task.** Different from the learning object on the *fixed* data  $X$  in Sec. 2.1, the performance of mixup classification is depending on the sub-task (a) because the mixup policies  $h(\cdot)$  and  $v(\cdot)$  reflect a certain relationship between the two classes (sub-manifolds). Therefore, we regard (b) as an auxiliary task to (a) and model  $h(\cdot)$  as a sub-network  $\mathcal{M}_\phi$  with the parameter  $\phi \in \Phi$ , called Mixer (see Sec. 3.3), to generate a pixel-wise mask  $s \in \mathbb{R}^{H \times W}$  for sample mixup. Intuitively, the mixup mask  $s_i$  is directly related to  $\lambda$  and the contents of  $(x_i, x_j)$ ,  $\mathcal{M}_\phi$  also takes  $l$ -th layer feature maps  $z^l \in \mathbb{R}^{C_l \times H_l \times W_l}$  as the input,  $\mathcal{M}_\phi : x_i, x_j, z_i^l, z_j^l, \lambda \mapsto x_m$ . The generation process of  $\mathcal{M}_\phi$  can be supervised by a mixup classification loss (see Sec. 3.2) as  $\mathcal{L}_\phi^{cls}$ , and a mask loss designed for generated mask  $s_i$  (see Sec. 3.3) denoted as  $\mathcal{L}_\phi^{mask}$ . Formally, we have the mixup generation loss as  $\mathcal{L}_\phi = \mathcal{L}_\phi^{cls} + \mathcal{L}_\phi^{mask}$ , and the final learning objective for SAMix is,

$$\min_{\theta, \omega, \phi} \mathcal{L}_{\theta, \omega} + \mathcal{L}_\phi. \quad (5)$$

Both  $\mathcal{L}_{\theta, \omega}$  and  $\mathcal{L}_\phi$  can be optimized alternatively in a unified framework using a momentum pipeline with the stop-gradient operation [15, 32], as shown in Figure 6 (left).

## 3. SAMix for Discriminative Representations

### 3.1. Instance-level Mixup Classification

**Cross-view training pipeline.** We begin by analyzing the learning objective of mixup classification sub-task. According to IB, the objective of class-level mixup classification is consistent with Eq. 1 as,  $\max_{\theta, \omega} I(z_m, y_m)$ . However, there are two possible objectives for instance-level mixup in Eq. 4: the *same-view*,  $\max_{\theta, \omega} \lambda I(z_m^{\tau_q}, z_i^{\tau_q}) + (1 - \lambda) I(z_m^{\tau_q}, z_j^{\tau_q})$ , and *cross-view* objective,  $\max_{\theta, \omega} \lambda I(z_m^{\tau_q}, z_i^{\tau_k}) + (1 - \lambda) I(z_m^{\tau_q}, z_j^{\tau_k})$ . As shown in Figure 3 (a), we hypothesize

that the cross-view objective yields better CL performance than the same-view because the mutual information between two augmented view should be reduced while keeping task-relevant information [43, 45]. To verify this hypothesis, we design an experiment of various mixup methods with  $\alpha = 1$  on STL-10 with ResNet-18 (detailed in Sec. 4.2 and A.2), as shown in Figure 3 (b), and conclude: (i) Degenerated solutions occur when use the same-view pipeline while using the cross-view pipeline outperforms the CL baseline. It is mainly caused by degenerated mixed samples which contain parts of the same view of two source images. Therefore, we propose the cross-view pipeline for the instance-level mixup, where  $z_i$  and  $z_j$  in Eq. 4 are representations of  $x_i^{T_k}$  and  $x_j^{T_k}$ . (ii) Combining both the original and mixup infoNCE loss,  $\ell^{NCE}(z_i^{T_q}, z_i^{T_k}) + \ell^{NCE}(z_m)$ , surpasses only using one of them, which indicates that mixup enables  $f_\theta$  to learn relationship between local neighborhood systems.

**Properties of mixup classification.** We then discuss the properties of instance-level mixup classification from two aspects: *inter-class* and *intra-class* mixup. In the case of class-level mixup, compared to the CE loss in Eq. 1, the mixup CE enhances the inter-class relationship as soft labels classification task while considering the intra-class relationship compact. In instance-level mixup, we hypothesize that the class information is still decisive for treating the inter- and intra-class relationship differently: *strong* inter-class mixup for discrimination and *weak* intra-class mixup for compactness. To verify the hypothesis, we conducted a CL experiment on Tiny-ImageNet (Tiny), which uses different intensities of inter- and intra-class mixup (detailed in A.2). Notice that mixed samples from CutMix [54] are more discriminative than MixUp [56] and using  $\alpha \in [0.2, 1, 2, 4]$  represents the mixup intensity from weak to strong. As shown in Figure 3 (c), the top performance is achieved by using MixUp with large  $\alpha$  as the intra-class mixup while CutMix with small  $\alpha$  as the inter-class, which supports our hypothesis.

### 3.2. Learning Objective for Mixup Generation

**Properties of mixup generation.** Asymmetric to the mixup classification, we decompose the objective of mixup generation into *local* and *global* terms, as shown in Table 1. We argue that mixup generation is aimed to *optimize the local term subject to the global term*. In the case of class-level mixup, for example, optimize  $(1 - \lambda)I(x_m, y_i) = \lambda I(x_m, y_j)$  (local) while  $I(x_m, y_c)$  is minimized for all classes  $c$  which are not belong to class  $y_i$  and  $y_j$  (global). Formally, assuming  $y_i$  and  $y_j$  belong to the class  $a$  and class  $b$ , we call the local term in Eq. 3 as parametric binary cross-entropy mixup loss (pBCE) for SL:

$$\ell_+^{CE}(p_m) = -\lambda y_{i,a} \log p_m - (1 - \lambda) y_{j,b} \log p_m, \quad (6)$$

where  $y_{i,a} = 1$  and  $y_{i,b} = 1$  denote the one-hot label for the class  $a$  and  $b$ . Notice that we use  $\ell_+$  and  $\ell_-$  to represent the local and global parts. Symmetrically, we have non-parametric binary cross-entropy mixup loss (BCE) for CL:

$$\ell_+^{NCE}(z_m) = \frac{\lambda z_m z_i}{z_m z_i + z_m z_j} + \frac{(1 - \lambda) z_m z_j}{z_m z_i + z_m z_j}, \quad (7)$$

According to IB, the global term serves as a constrain to compress the task-irrelevant information in  $x_m$ . We verify the *necessity* of this global constrain by visualization the top-1 and top-2 accuracy on mixed data with  $\lambda \in [0, 1]$  in Figure 4. Notice that the generation objective in PuzzleMix [26] is to maximize the saliency information of  $x_i$  and  $x_j$  in  $x_m$ , which is similar to the pBCE loss. Obviously, using the mixup CE loss as the objective for Mixer (see Sec. 3.3) yields better global discrimination than using the pBCE loss.

Property	Instance-level mixup	Class-level mixup
Local	$(1 - \lambda)I(x_m^*, x_i) = \lambda I(x_m^*, x_j)$	$(1 - \lambda)I(x_m^*, y_i) = \lambda I(x_m^*, y_j)$
Global	$I(x_m^*, x_k) = 0, \forall k, k \neq i, k \neq j.$	$I(x_m^*, y_c) = 0, \forall c, y_c \neq y_i, y_c \neq y_j.$

Table 1. Properties of learning objectives of mixup generation.

**Objective for mixup generation.** Since both the local and global terms contribute to mixup generation, we discuss the importance of each term in the SL and SSL tasks to design a balanced learning objective. We first analyze the properties of both terms with two hypothesizes: (i) the local term  $\ell_+$  *determines* the generation performance, (ii) the global term  $\ell_-$  *improves* global discrimination but is sensitive to class information. To verify these properties, we design an empirical experiment based on the proposed Mixer on Tiny (detailed in A.2). Notice that the main difference between the mixup CE (Eq. 3) and infoNCE (Eq. 4) is whether to adopt parametric class centroids. Therefore, we compare the intensity of class information among unlabeled (UL), pseudo labels (PL), and ground truth labels (L). Notice that PL is generated by ODC [55] with the cluster number  $C$  and the class supervision can be imported to mixup infoNCE loss by filtering out negative samples with PL or L as [24]

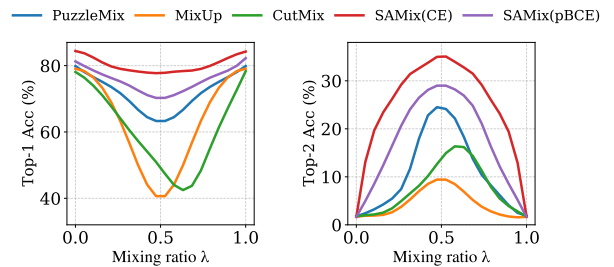


Figure 4. Left: Top-1 accuracy of mixed data on CIFAR-100. Prediction is counted as correct if the top-1 prediction belongs to  $\{y_i, y_j\}$ . Right: Top-2 accuracy of mixed data. Prediction is counted as correct if the top-2 predictions are equal to  $\{y_i, y_j\}$ .



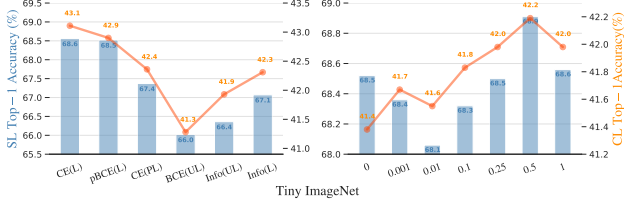


Figure 5. Analysis of the learning objective of Mixer on Tiny ImageNet with ResNet-18. The left figure shows results of various losses on the SL task (left y axis) and the CL task (right y axis). The right one shows the effect of using various negative weights  $\eta$ .

denoted as infoNCE (L) and infoNCE (PL). As shown in the left of Figure 5, our hypotheses are verified in the SL task (as the performance decreases from CE(L) to pBCE(L) and CE(PL) losses), but the opposite result appears in the CL task. The performance increases from InfoNCE(UL) to InfoNCE(L) as the false negative samples are removed [24, 38] while trivial solutions occur using BCE(UL) (as shown in Figure 7). We argue that the local objective of instance-level mixup relies heavily on its global constrain while the global constrain depends on class information. Thus, we propose it is better to explicitly import class information as PL for instance-level mixup to generate "strong" inter-class mixed samples while preserving intra-class compactness. Practically, we provide two versions of the learning objective: mixup CE loss in Eq. 3 with PL as clustering version (SAMix-C), mixup infoNCE loss in Eq. 4 as infoNCE version (SAMix-I). We verify the MI between  $x_m$  and  $x_i$  v.s. the given  $\lambda$  for the instance-level mixup in Figure 8 (d), which shows mixed samples from SAMix-C contain more task-relevant information than SAMix-I.

**$\eta$ -balanced mixup loss.** Then, we hypothesize that the best performing mixed samples will be close to the sweet spot: achieving  $\lambda$  smoothness locally between two classes or neighborhood systems while globally discriminating from other classes or instances. We propose an  $\eta$ -balanced mixup loss as the objective of mixup generation,

$$\ell_\eta = \ell_+ + \eta \ell_-, \quad \eta \in [0, 1]. \quad (8)$$

We analyze the performance of using various  $\eta$  in Eq. 8 on Tiny, as shown in the right of Figure 5, and find that using  $\eta = 0.5$  performs best on both the SL and CL tasks. In the end, we provide the learning objective,  $\mathcal{L}_\phi^{cls} \triangleq \ell_+^{CE} + \eta \ell_-^{CE}$ , with L for class-level mixup and with PL for SAMix-C,  $\mathcal{L}_\phi^{cls} \triangleq \ell_+^{NCE} + \eta \ell_-^{NCE}$  for SAMix-I (detailed in A.1).

### 3.3. Mixer for Mixup Generation

Inspired by self-attention mechanism [50], we design Mixer  $\mathcal{M}_\phi$  to solve three sub-problems: (a) how to encode the mixing ratio  $\lambda$ , (b) how to model the mixup relationship between two samples, and (c) how to encode the prior knowledge of mixup.

**Adaptive  $\lambda$  encoding and mixing attention.** Since mixup generation is directly guided by the randomly sampled mixing ratio  $\lambda$ , the predicted mask should be proportional to  $\lambda$ . Here, we regard  $\lambda$  as the prior knowledge and propose an *adaptive  $\lambda$  encoding* as,  $z_{i,\lambda}^l = (1 + \gamma\lambda)z_i^l$ , where  $\gamma$  is a learnable scalar that constrained to  $[0, 1]$ . Symmetrically, we have  $z_{j,1-\lambda}^l = (1 + \gamma(1 - \lambda))z_j^l$ . Notice that  $\gamma$  is initialized to 0 during training. Then, Mixer models the mixing relationship between  $z_{i,\lambda}^l$  and  $z_{j,1-\lambda}^l$  using self-attention and predicts  $s_i$  by three steps: (1) it models the content of  $z_i$  by a sub-module,  $C_i = \mathcal{C}(z_i)$ , where  $C_i \in \mathbb{R}^{H_i \times W_i}$  is a 2D tensor like the final mask  $s_i$ . (2) it computes the mixing relationship between two samples using a new *mixing attention*: we concatenate  $(z_{i,\lambda}^l, z_{j,1-\lambda}^l)$  as the input,  $\tilde{z}^l = \text{concat}(z_{i,\lambda}^l, z_{j,1-\lambda}^l)$ , and compute the attention weight as,  $P_{i,j} = \text{softmax}(\frac{(W_P \tilde{z}^l)^T \otimes W_P \tilde{z}^l}{\mathcal{N}(\tilde{z}^l)})$ , where  $\mathcal{N}(\tilde{z}^l)$  denotes a normalization factor and  $\otimes$  is matrix multiplication. Notice that the mixing attention provides both the cross-attention between  $z_{i,\lambda}^l$  and  $z_{j,1-\lambda}^l$  and the self-attention of each feature itself. (3) it predicts the probability of each coordinate belonging to  $x_i$  as,  $s_i = U(\sigma(P_{i,j} \otimes C_i))$ , where  $U(\cdot)$  is an upsampling and  $\sigma(\cdot)$  denotes sigmoid activation.

**Non-linear content modeling.** In common cases, the content sub-module  $\mathcal{C}$  is a linear projection in self-attention,  $C_i = W_z \tilde{z}^l$ , where  $W_z$  denotes a  $1 \times 1$  convolution. However, we find the training process of Mixer is unstable with the linear  $\mathcal{C}$  in the early period and sometimes trapped in trivial solutions (especially in SSL tasks), such as all coordinates on  $s_i$  predicted as a constant. As shown in A.2, we visualize  $C_i$  and  $P_{i,j}$  to compare trivial results with some non-trivial ones, and find that the constant  $s_i$  is usually caused by a constant  $C_i$ . We hypothesize that trivial solutions happen earlier in the linear  $\mathcal{C}$  than in  $P_{i,j}$ , which linearly projects the high-dimensional feature to 1-dim. Hence, we design a

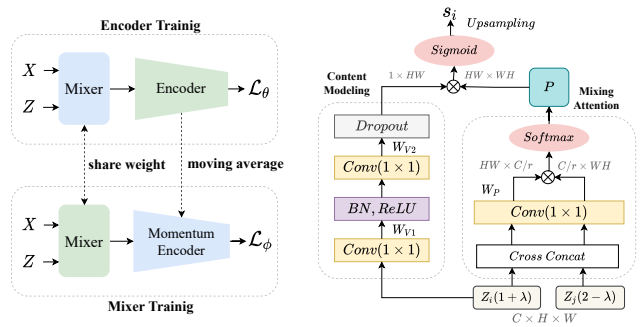


Figure 6. Overall training framework of SAMix (left) and network architecture of Mixer  $\mathcal{M}_\phi$  (right).  $X$  and  $Z$  denote the input sample and corresponding feature maps from Momentum Encoder. The blue modules on the left are not updated by the back-propagation in the dashed box. That means the two parallel pipelines optimize Mixer and Encoder alternatively, and update each other's frozen modules by weight sharing and moving average (see A.1.2).

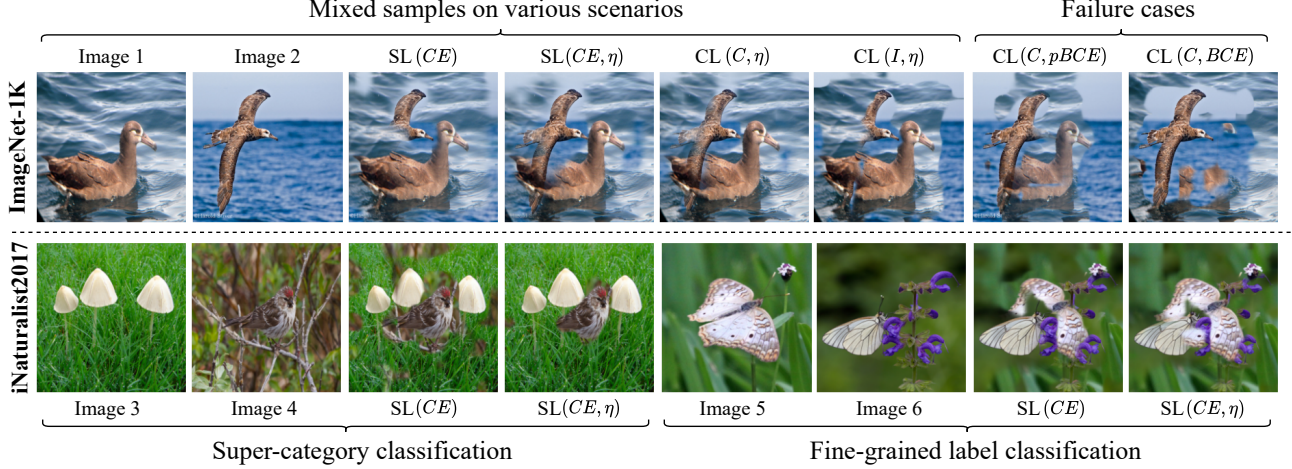


Figure 7. Visualization and comparison of mixed samples from Mixer in various learning scenarios on IN-1k and iNat2017. Note that  $\lambda = 0.5$  and  $\eta = 0.5$  if the balance coefficient  $\eta$  is included. CL(C) and CL(I) denote using SAMix-C and SAMix-I separately.

*non-linear content modeling* sub-module  $\mathcal{C}_{NC}$  that contains two  $1 \times 1$  convolution layers with a batch normalization layer and a ReLU layer in between, as shown in Figure 6 (left). To increase the robustness and randomness of mixup training, we add a Dropout layer with a dropout ratio of 0.1 in  $\mathcal{C}_{NC}$ . Formally, Mixer  $\mathcal{M}_\phi$  can be written as,

$$s_i = U \left( \sigma \left( \text{softmax} \left( \frac{(W_P \tilde{z}^l)^T \otimes W_P \tilde{z}^l}{N(\tilde{z}^l)} \right) \otimes \mathcal{C}_{NC}(z_{i,\lambda}^l) \right) \right). \quad (9)$$

**Prior knowledge of mixup.** Moreover, we summarize some prior knowledge commonly adopted in input space mixup as two aspects: (a) adjusting the mean of  $s_i$  correlated with  $\lambda$ , and (b) balancing the smoothness of local image patches while maintaining discrimination of  $x_m$ . As for the first aspect, a mask loss is introduced to align the mean of  $s_i$  to  $\lambda$ ,  $\ell_{mean} = \beta \max(|\lambda - \mu_i| - \epsilon, 0)$ , where  $\mu_i = \frac{1}{HW} \sum_{h,w} s_{i,h,w}$  is the mean and  $\epsilon = 0.1$  as a margin. Meanwhile, we propose a test time  $\lambda$  adjusting method. Assuming  $\mu_i < \lambda$ , we adjust each coordinate on  $s_i$  as  $\hat{s}_i = \frac{\mu_i}{\lambda} s_i$ , and  $\hat{s}_j = 1 - \hat{s}_i$ . As for the second aspect, we adopt a bilinear upsampling as  $U(\cdot)$  for smoother masks and propose a variance loss to encourage the sparsity of learned masks,  $\ell_{var} = \frac{1}{WH} \sum_{w,h} (\mu_i - s_{w,h})^2$ . Finally, we summarize the mask loss as,  $\mathcal{L}_\phi^{mask} = \beta(\ell_{mean} + \ell_{var})$ , where  $\beta$  is a balancing weight. We initialize  $\beta$  to 0.1 and linearly decrease to 0 during training.

### 3.4. Discussion and Visualization of SAMix

To show the influence of local and global constraints on mixup generation, we visualize mixed samples that are generated from Mixer on various scenarios in Figure 7.

**Class-level.** In the supervised classification task, global constraint localizes key features by discriminating to other classes, while local term is prone to preserve more information related to current two samples and classes. For example,

comparing the mixed results with and without  $\eta$ -balanced mixup loss, it was found that pixels of the foreground target was of interest to Mixer. When the global constraint is balanced ( $\eta = 0.5$ ), the foreground target is retained more completely. Importantly, our designed Mixer remains invariant to the background for the more challenging fine-grained classification and preserves discriminative features.

**Instance-level.** Since no label supervisions are available for SSL, the global and local terms are transformed from class to instance. Similar results are shown in the top row, the only difference is that SAMix-C has a more precise target correspondence compared to SAMix-I via introducing class information by PL, which further indicates the importance of the information of classes. If we only focus on local relationships, Mixer can only generate mixed samples with fixed patterns (the last two results in the top row). These failure cases imply the effect of global constraints.

## 4. Experiments

We first evaluate SAMix for supervised learning (SL) in Sec. 4.1 and self-supervised learning (SSL) in Sec. 4.2, and then perform ablation studies in Sec. 4.3. Six benchmarks are used for evaluation: CIFAR-100 [28], Tiny-ImageNet (Tiny) [8], ImageNet-1k (IN-1k) [39], STL-10 [10], CUB-200 [49], FGVC-Aircraft (Aircraft) [34], and iNaturalist2017 (iNat2017) [22]. All experiments are conducted with PyTorch and reported the *mean of 3 trials*. SAMix uses  $\alpha = 2$  and the feature layer  $l = 3$  for all datasets.

### 4.1. Evaluation on Supervised Image Classification

This subsection evaluates the performance gain of SAMix for fine-grained, small- and large-scale image classification tasks. We adopt ResNet [19] (R) and ResNeXt(32x4d) (RX) [53] as backbone networks. We use SGD optimizer with cosine scheduler [33] for all SL experiments. For a fair

Method	Tiny		IN-1k			
	R-18	RX-50	R-18	R-34	R-50	R-101
Vanilla	61.68	65.04	71.83	75.29	77.35	78.91
MixUp	63.86	66.36	71.72	75.73	78.44	80.60
CutMix	65.53	66.47	70.03	75.16	78.69	80.59
ManifoldMix	64.15	67.30	71.73	75.44	78.21	80.64
SaliencyMix	64.60	66.55	70.21	75.01	78.46	80.45
FMix*	63.47	65.08	70.30	75.12	78.51	80.20
PuzzleMix	65.81	66.92	71.64	75.84	78.87	80.67
Co-Mixup	66.29	67.31	71.73	75.89	78.92	80.69
ResizeMix*	63.74	65.87	71.32	75.64	78.91	80.52
AutoMix*	<b>67.33</b>	<b>70.72</b>	<b>72.05</b>	<b>76.10</b>	<b>79.25</b>	<b>80.98</b>
<b>SAMix</b>	<b>68.89</b>	<b>72.18</b>	<b>72.33</b>	<b>76.35</b>	<b>79.41</b>	<b>81.08</b>
Gain	+1.56	+1.46	+0.28	+0.25	+0.16	+0.10

Table 2. Top-1 accuracy (%) of supervised image classification on Tiny and IN-1k.

CL baseline	mixup method	R18		R50	
		400ep	800ep	400ep	800ep
MoCo.V2	-	81.50	85.64	84.89	89.68
	MixUp	<b>84.51</b>	<b>87.93</b>	<b>88.24</b>	<b>92.20</b>
	ManifoldMix	84.17	87.70	88.06	91.65
	CutMix	84.28	87.60	87.51	90.81
	SaliencyMix	84.33	87.27	87.35	90.77
	FMix*	84.43	87.68	88.14	91.56
	ResizeMix*	83.88	87.25	86.88	90.83
	<b>SAMix-I</b>	<b>85.44</b>	<b>88.58</b>	<b>88.87</b>	<b>92.41</b>
SwAV <sup>†</sup> (C)	-	81.10	85.56	84.35	88.79
MoCo.V2 (C)	Inter-Intra*	84.89	87.85	88.33	92.24
MoCo.V2 (C)	PuzzleMix*	<b>84.98</b>	<b>88.07</b>	<b>88.40</b>	91.98
MoCo.V2 (C)	<b>SAMix-C</b>	<b>85.60</b>	<b>88.63</b>	<b>88.91</b>	<b>92.45</b>

Table 3. Top-1 accuracy (%) of linear classification on STL-10 with 400 and 800-epoch.

CL method	mixup method	Tiny		IN-1k	
		R18	R50	R18	R50
MoCo.V2	-	38.29	42.08	52.85	67.66
MoCo.V2	MixUp	41.24	46.61	53.03	68.07
MoCo.V2	CutMix	41.62	46.24	52.98	68.28
MoCo.V2	SaliencyMix	41.14	46.13	53.06	68.31
MoCo.V2	FMix*	41.09	46.30	53.10	68.42
MoCo.V2 (C)	PuzzleMix*	41.86	46.72	53.46	68.48
MoChi <sup>†</sup>	input+latent	41.78	46.55	53.12	68.01
i-Mix <sup>†</sup>	input+latent	41.61	46.57	53.09	68.10
UnMix <sup>†</sup>	input+latent	-	-	-	68.60
WBSIM <sup>‡</sup>	input	-	-	-	68.40
MoCo.V2	<b>SAMix-I</b>	<b>41.97</b>	<b>47.23</b>	<b>53.75</b>	<b>68.79</b>
MoCo.V2 (C)	<b>SAMix-C</b>	<b>43.68</b>	<b>47.51</b>	<b>53.93</b>	<b>68.86</b>

Table 4. Top-1 accuracy (%) of linear classification on Tiny and IN-1k.

comparison, grid search is performed for hyper-parameters  $\alpha \in \{0.2, 0.5, 1.0, 2.0, 4.0\}$  of all mixup methods. We use  $\alpha = 1$  and follow other hyper-parameters the original paper by default. Notice that \* denotes unpublished work on arxiv. Following [32], momentum training coefficient is gradually increased from 0.999 to 1 in a cosine curve by default. The *median* of validation results in the last 10 training epochs is recorded for each trial.

**Setups** For a fair comparison, we adopt the following basic training settings identically for all methods in SL tasks. We adopt *RandomFlip* and *RandomCrop* with 4 pixels reflect padding as basic data augmentations for CIFAR-100 while *RandomFlip* and *RandomResizedCrop* for other datasets. For CIFAR-100, the SGD weight decay is 0.0001, momentum is 0.9, initial learning rate  $lr = 0.1$ , and train 800 epochs with the batch size of 100. For Tiny, we train 400 epochs with the initial learning rate  $lr = 0.2$  and the batch size of 100. For IN-1k, the total epoch is 300 with the initial learning rate  $lr = 0.1$  and the batch size of 256. For small-scale fine-grained classification tasks on CUB-200 and Aircraft, we use pre-trained models on IN-1k provided by PyTorch [35] as initialization, and train 200 epochs with the initial learning rate  $lr = 0.001$ , the weight decay 0.0005, and the batch size of 16. For the large scale fine-grained recognition task on iNat2017, we train 100 epochs with  $lr = 0.1$ .

**Comparison and discussion** On the small-scale and fine-grained classification tasks, as shown in Table 5, SAMix consistently improves the classification performance over the previous best algorithm AutoMix on CIFAR-100, CUB-200, and Aircraft by improving the design of Mixer. Notice that SAMix significantly improved the performance of CUB-200 and Aircraft by 1.24% and 0.78% based on ResNet-18, and continued to expand its dominance on Tiny by bringing 1.23% and 1.40% improvement on ResNet-18 and ResNeXt-50. As for the large-scale classification task, SAMix also outperforms all existing methods on IN-1k. Specially, SAMix improves the second best method by 0.25% with ResNet-50.

## 4.2. Evaluation on Self-supervised Learning

In this subsection, we evaluate SAMix on SSL tasks pre-training on STL-10, Tiny, and IN-1k. All comparing meth-

ods are based on MoCo.V2 excepts SwAV [4]. We adopt all the hyper-parameter configurations from MoCo.V2 for pre-training on these datasets unless otherwise stated. We compared SAMix in two dimensions in CL: (i) compare with other mixup variants, based on our proposed cross-view pipeline, and the predefined cluster information is given (denotes by C) or not, as shown in Table 3. (ii) longitudinal comparison with CL methods that utilize *input space* (i.e., Mixup and CutMix) and *input+latent* space mixup strategies, including MoChi [23], i-Mix [30], Un-Mix [41] and WBSIM [9], as shown in Table 4. Notice that \* denotes our modified methods (PuzzleMix\* uses PL and Inter-Intra\* combines inter-class CutMix with intra-class MixUp in Sec. 3), † denotes reproduced results by official source code, ‡ denotes original reported results, and other results are reproduced by us (see A.1).

**Linear Classification** Following the linear classification protocol proposed in MoCo, we train a linear classifier on the top of frozen backbone features with the supervised train set. We train 100 epochs using SGD with a batch size of 256. The initialized learning rate is set to 0.1 for Tiny and STL-10 while 30 for IN-1k, and decay by 0.1 at epoch 30 and 60. As shown in Table 3, SAMix-I outperforms all the linear mixup methods by a large margin while SAMix-C surpasses the saliency-based PuzzleMix when PL is available. Meanwhile, Table 4 demonstrates that both SAMix-I and SAMix-C surpass other CL methods combined with the predefined mixup. Overall, SAMix-C yields best performance

Method	CIFAR-100		CUB-200		FGVC-Aircraft		iNat2017	
	R-18	RX-50	R-18	RX-50	R-18	RX-50	R-50	RX-101
Vanilla	78.04	81.09	77.68	83.01	80.23	85.10	60.23	63.70
MixUp	79.12	82.10	78.39	84.58	79.52	85.18	61.22	66.27
CutMix	78.17	78.32	78.40	85.68	78.84	84.55	62.34	67.59
ManifoldMix	80.35	82.88	79.76	86.38	80.68	86.60	61.47	66.57
SaliencyMix	79.12	78.77	77.95	83.29	80.02	84.31	62.51	67.20
FMix*	79.69	79.02	77.28	84.06	79.36	84.85	61.90	66.64
PuzzleMix	80.43	82.57	78.63	84.51	80.76	86.23	62.66	67.72
ResizeMix*	80.01	79.73	78.50	84.77	78.10	84.08	62.29	66.82
AutoMix*	<b>82.04</b>	<b>83.64</b>	<b>79.87</b>	<b>86.56</b>	<b>81.37</b>	<b>86.69</b>	<b>62.97</b>	<b>67.87</b>
<b>SAMix</b>	<b>82.30</b>	<b>84.11</b>	<b>81.11</b>	<b>86.83</b>	<b>82.15</b>	<b>86.80</b>	<b>63.32</b>	<b>68.36</b>
Gain	+0.26	+0.47	+1.24	+0.27	+0.78	+0.11	+0.35	+0.48

Table 5. Top-1 accuracy (%) of supervised image classification on CIFAR-100, CUB-200, Aircraft, and iNat2017.



in CL takes which indicates it provides more task-relevant information with the help of class information in PL.

**Downstream Tasks** Following the transfer learning protocol in MoCo, we evaluate transferable abilities of the learned representation of comparing methods to object detection task on PASCAL VOC [13] and COCO [31] in Detec-tron2 [52]. In Table 6, we fine-tune Faster R-CNN [37] with R50-C4 backbone with pre-trained models on VOC *train-val07+12* and evaluate on the VOC *test2007* set. Similarly, Mask R-CNN [18] is fine-tuned ( $2\times$  schedule) on the COCO *train2017* and evaluated on the COCO *val2017* set.

CL Method	mixup method	Faster R-CNN			Mask R-CNN		
		AP	AP <sub>50</sub>	AP <sub>75</sub>	AP <sup>b</sup>	AP <sub>50</sub> <sup>b</sup>	AP <sub>75</sub> <sup>b</sup>
MoCo.V2	-	56.9	82.2	63.4	40.6	60.1	44.0
MoCo.V2	Mixup	57.4	82.5	64.0	41.0	60.8	44.3
MoCo.V2	CutMix	57.3	82.7	64.1	41.1	60.8	44.4
MoChi <sup>†</sup>	<i>input+latent</i>	57.1	82.7	64.1	41.0	60.8	<b>44.5</b>
i-Mix <sup>†</sup>	<i>input+latent</i>	57.5	82.7	64.2	-	-	-
UnMix <sup>‡</sup>	<i>input+latent</i>	<b>57.7</b>	<b>83.0</b>	<b>64.3</b>	<b>41.2</b>	<b>60.9</b>	<b>44.7</b>
WBSIM <sup>‡</sup>	<i>input</i>	57.4	82.8	64.2	40.7	60.8	44.2
MoCo.V2	<b>SAMix-C</b>	<b>57.8</b>	<b>83.1</b>	<b>64.4</b>	<b>41.3</b>	<b>61.1</b>	<b>44.7</b>

Table 6. Transferring to object detection with Faster R-CNN on VOC07+12 and Mask R-CNN on COCO2017.

### 4.3. Ablation Study

We conduct ablation studies in five aspects: (i) **Mixer**: Table 8 verifies the effectiveness of each proposed module in both SL and CL tasks on Tiny. The first three modules enable Mixer to model the non-linear mixup relationship, while the next two modules enhance Mixer especially in CL tasks. (ii) **Learning objectives**: We analyze the effectiveness of proposed  $\ell_\eta$  with other losses, as shown in Table 7. Using  $\ell_\eta$  for the mixup CE and infoNCE consistently improves the performance both for the CL task on STL-10 and Tiny. (iii) **Time complexity analysis**: Figure 8 (c) shows computational analysis conducted on the SL task on IN-1k using 100-epochs protocol [51]. It reflects that the overall accuracy v.s. time efficiency of SAMix is superior in contrast to other methods. (iv) **Hyper-parameter**: Figure 8 (a) and (b) show ablation results of the hyper-parameter  $\alpha$  and the clustering number  $C$  for SAMix-C. We empirically choose  $\alpha=2.0$  and  $C=200$  as default. (v) **MI of mixup**: Figure 8 (d) shows estimated  $I(x_m, x_i)$  on Tiny by MINE [1] (detailed in A.2), which indicates SAMix-C provides more task-relevant information than SAMix-I and other methods.

method	STL-10	Tiny	module	SL	CL
BCE	85.25	41.28	Mixing attention	67.17	40.58
infoNCE	85.36	41.85	+Adaptive $\lambda$	67.95	41.82
infoNCE ( $\eta = 0.5$ )	<b>85.44</b>	<b>41.97</b>	+Non-linear content	68.36	42.35
CE (PL)	85.56	42.36	+ $\mathcal{L}_{mask}$	68.49	42.57
CE (PL)+infoNCE	85.41	42.12	+ $\lambda$ adjusting	68.61	43.14
CE (PL, $\eta = 0.5$ )	<b>85.60</b>	<b>42.53</b>	+ $\ell_\eta$ ( $\eta = 0.5$ )	<b>68.89</b>	<b>43.68</b>

Table 7. Ablation of the proposed learning objectives in the SSL task on STL-10 and Tiny.

Table 8. Ablation of proposed modules in Mixer and the  $\eta$ -balanced loss on Tiny.

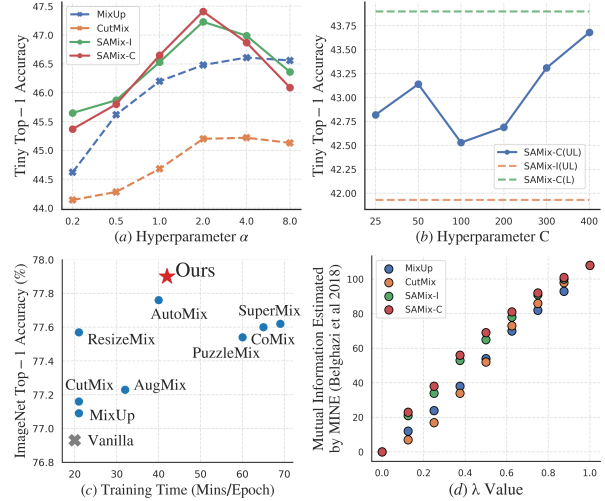


Figure 8. Ablation of SAMix. (a) hyper-parameter  $\alpha$  for mixup (b) the cluster number  $C$  for SAMix-C in CL tasks on Tiny, (c) top-1 accuracy v.s. training time on IN-1k based on ResNet-50 with 100 epochs, and (d) estimated MI v.s. mixing ratio  $\lambda$  on Tiny.

## 5. Related Work

**Mixup of class level** There are three types of class-level mixup: linear mixup of input space [16, 21, 36, 54, 56] and latent space [14, 48], saliency-based [25, 26, 46], and learning mixup generation and classification end-to-end [11, 32]. SAMix belongs to the third type and learns both class- and instance-level mixup relationships. See A.5 for details.

**Mixup of instance level** A complementary method for better instance-level representation learning is to apply mixup in SSL scenarios. Most approaches are limited to linear mixup methods, such as using MixUp and CutMix in the input space or latent space mixup [41] for SSL without ground-truth labels. MoChi [23] propose mixing the negative sample in the embedding space to increase the number of hard negatives to improve CL. i-Mix [30] and BSIM [9] demonstrated how to regularize CL by mixing instances in input/latent spaces. We introduce SAMix for SSL, which adaptively learns the mixup policy online.

## 6. Limitations and Discussion

In this work, with the motivation of designing a scenario-agnostic mixup framework, we study the objective of mixup generation as a local-emphasized and global-constrained sub-task for learning adaptive mixup policy at both in class and instance level. SAMix provides a unified framework for improving discriminative representation learning based on our proposed learnable Mixer and cross-view pipeline. As limitations, the Mixer only takes two samples as input and conflicts when the task-relevant information is overlapping. In the future, more than two samples or conflict-aware Mixer is another promising avenue for future research.



## References

- [1] Mohamed Ishmael Belghazi, Aristide Baratin, Sai Rajeswar, Sherjil Ozair, Yoshua Bengio, Aaron Courville, and R Devon Hjelm. Mine: Mutual information neural estimation. In *Proceedings of the International Conference on Machine Learning (ICML)*, 2018. [8](#), [14](#)
- [2] Yoshua Bengio, Aaron Courville, and Pascal Vincent. Representation learning: A review and new perspectives. *IEEE transactions on pattern analysis and machine intelligence*, 35(8):1798–1828, 2013. [1](#)
- [3] Mathilde Caron, Piotr Bojanowski, Armand Joulin, and Matthijs Douze. Deep clustering for unsupervised learning of visual features. In *Proceedings of the European Conference on Computer Vision (ECCV)*, 2018. [12](#)
- [4] Mathilde Caron, Ishan Misra, Julien Mairal, Priya Goyal, Piotr Bojanowski, and Armand Joulin. Unsupervised learning of visual features by contrasting cluster assignments. In *Advances in Neural Information Processing Systems (NeurIPS)*, 2020. [7](#), [13](#), [15](#)
- [5] Ting Chen, Simon Kornblith, Mohammad Norouzi, and Geoffrey Hinton. A simple framework for contrastive learning of visual representations. In *Proceedings of the International Conference on Machine Learning (ICML)*, 2020. [1](#), [3](#), [15](#)
- [6] Xinlei Chen, Haoqi Fan, Ross Girshick, and Kaiming He. Improved baselines with momentum contrastive learning. *arXiv preprint arXiv:2003.04297*, 2020. [12](#)
- [7] Xinlei Chen, Haoqi Fan, Ross Girshick, and Kaiming He. Improved baselines with momentum contrastive learning. *arXiv preprint arXiv:2003.04297*, 2020. [15](#)
- [8] Patryk Chrabaszcz, Ilya Loshchilov, and Frank Hutter. A downsampled variant of imagenet as an alternative to the cifar datasets. *arXiv preprint arXiv:1707.08819*, 2017. [6](#), [12](#)
- [9] Xiangxiang Chu, Xiaohang Zhan, and Xiaolin Wei. Beyond single instance multi-view unsupervised representation learning. *arXiv preprint arXiv:2011.13356*, 2020. [7](#), [8](#), [15](#)
- [10] Adam Coates, Andrew Ng, and Honglak Lee. An analysis of single-layer networks in unsupervised feature learning. In *Proceedings of the fourteenth international conference on artificial intelligence and statistics*, pages 215–223. JMLR Workshop and Conference Proceedings, 2011. [6](#), [12](#)
- [11] Ali Dabouei, Sobhan Soleymani, Fariborz Taherkhani, and Nasser M Nasrabadi. Supermix: Supervising the mixing data augmentation. In *Proceedings of the IEEE/CVF Conference on Computer Vision and Pattern Recognition*, pages 13794–13803, 2021. [1](#), [8](#), [15](#)
- [12] Jacob Devlin, Ming-Wei Chang, Kenton Lee, and Kristina Toutanova. Bert: Pre-training of deep bidirectional transformers for language understanding. *arXiv preprint arXiv:1810.04805*, 2018. [1](#)
- [13] Mark Everingham, Luc Van Gool, Christopher KI Williams, John Winn, and Andrew Zisserman. The pascal visual object classes (voc) challenge. *International journal of computer vision*, 88(2):303–338, 2010. [8](#), [12](#)
- [14] Mojtaba Faramarzi, Mohammad Amini, Akilesh Badri-naaraayanan, Vikas Verma, and Sarath Chandar. Patchup: A regularization technique for convolutional neural networks. *arXiv preprint arXiv:2006.07794*, 2020. [8](#), [15](#)
- [15] Jean-Bastien Grill, Florian Strub, Florent Altché, Corentin Tallec, Pierre H Richemond, Elena Buchatskaya, Carl Doersch, Bernardo Avila Pires, Zhaohan Daniel Guo, Mohammad Gheshlaghi Azar, et al. Bootstrap your own latent: A new approach to self-supervised learning. In *Advances in Neural Information Processing Systems (NeurIPS)*, 2020. [1](#), [3](#), [12](#), [15](#)
- [16] Ethan Harris, Antonia Marcu, Matthew Painter, Mahesan Niranjan, and Adam Prügel-Bennett Jonathon Hare. Fmix: Enhancing mixed sample data augmentation. *arXiv preprint arXiv:2002.12047*, 2(3):4, 2020. [8](#), [12](#), [15](#)
- [17] Kaiming He, Haoqi Fan, Yuxin Wu, Saining Xie, and Ross Girshick. Momentum contrast for unsupervised visual representation learning. In *Proceedings of the IEEE/CVF Conference on Computer Vision and Pattern Recognition*, pages 9729–9738, 2020. [1](#), [2](#), [13](#), [15](#)
- [18] Kaiming He, Georgia Gkioxari, Piotr Dollár, and Ross Girshick. Mask r-cnn. In *Proceedings of the International Conference on Computer Vision (ICCV)*, 2017. [8](#), [13](#)
- [19] Kaiming He, Xiangyu Zhang, Shaoqing Ren, and Jian Sun. Deep residual learning for image recognition. In *Proceedings of the IEEE conference on computer vision and pattern recognition*, pages 770–778, 2016. [6](#)
- [20] Kaiming He, Xiangyu Zhang, Shaoqing Ren, and Jian Sun. Deep residual learning for image recognition. In *Proceedings of the IEEE conference on computer vision and pattern recognition*, pages 770–778, 2016. [13](#)
- [21] Dan Hendrycks, Norman Mu, Ekin D Cubuk, Barret Zoph, Justin Gilmer, and Balaji Lakshminarayanan. Augmix: A simple data processing method to improve robustness and uncertainty. *arXiv preprint arXiv:1912.02781*, 2019. [8](#), [12](#)
- [22] Grant Van Horn, Oisin Mac Aodha, Yang Song, Yin Cui, Chen Sun, Alex Shepard, Hartwig Adam, Pietro Perona, and Serge Belongie. The inaturalist species classification and detection dataset. In *Proceedings of the Conference on Computer Vision and Pattern Recognition (CVPR)*, 2018. [6](#), [12](#)
- [23] Yannis Kalantidis, Mert Bulent Sariyildiz, Noe Pion, Philippe Weinzaepfel, and Diane Larlus. Hard negative mixing for contrastive learning. In *Advances in Neural Information Processing Systems (NeurIPS)*, 2020. [1](#), [7](#), [8](#), [15](#)
- [24] Prannay Khosla, Piotr Teterwak, Chen Wang, Aaron Sarna, Yonglong Tian, Phillip Isola, Aaron Maschinot, Ce Liu, and Dilip Krishnan. Supervised contrastive learning. In *Advances in Neural Information Processing Systems (NeurIPS)*, 2020. [4](#), [5](#)
- [25] Jang-Hyun Kim, Wonho Choo, Hosan Jeong, and Hyun Oh Song. Co-mixup: Saliency guided joint mixup with super-modular diversity. *arXiv preprint arXiv:2102.03065*, 2021. [1](#), [8](#), [12](#), [15](#)
- [26] Jang-Hyun Kim, Wonho Choo, and Hyun Oh Song. Puzzle mix: Exploiting saliency and local statistics for optimal mixup. In *International Conference on Machine Learning*, pages 5275–5285. PMLR, 2020. [1](#), [3](#), [4](#), [8](#), [12](#), [15](#)
- [27] Bruno Korbar, Du Tran, and Lorenzo Torresani. Cooperative learning of audio and video models from self-supervised synchronization. *arXiv preprint arXiv:1807.00230*, 2018. [1](#)
- [28] Alex Krizhevsky, Geoffrey Hinton, et al. Learning multiple layers of features from tiny images. 2009. [6](#), [12](#)

- [29] Alex Krizhevsky, Ilya Sutskever, and Geoffrey E Hinton. Imagenet classification with deep convolutional neural networks. In *Advances in neural information processing systems*, pages 1097–1105, 2012. 12
- [30] Kibok Lee, Yian Zhu, Kihyuk Sohn, Chun-Liang Li, Jinwoo Shin, and Honglak Lee. I-mix: A domain-agnostic strategy for contrastive representation learning. In *International Conference on Learning Representations (ICLR)*, 2021. 1, 7, 8, 15
- [31] Tsung-Yi Lin, Michael Maire, Serge Belongie, James Hays, Pietro Perona, Deva Ramanan, Piotr Dollár, and C Lawrence Zitnick. Microsoft coco: Common objects in context. In *Proceedings of the European Conference on Computer Vision (ECCV)*, 2014. 8, 12
- [32] Zicheng Liu, Siyuan Li, Di Wu, Zhiyuan Chen, Lirong Wu, Jianzhu Guo, and Stan Z Li. Automix: Unveiling the power of mixup. *arXiv preprint arXiv:2103.13027*, 2021. 3, 7, 8, 12, 15
- [33] Ilya Loshchilov and Frank Hutter. Sgdr: Stochastic gradient descent with warm restarts. *arXiv preprint arXiv:1608.03983*, 2016. 6
- [34] Subhransu Maji, Esa Rahtu, Juho Kannala, Matthew Blaschko, and Andrea Vedaldi. Fine-grained visual classification of aircraft. *arXiv preprint arXiv:1306.5151*, 2013. 6, 12
- [35] Adam Paszke, Sam Gross, Francisco Massa, Adam Lerer, James Bradbury, Gregory Chanan, Trevor Killeen, Zeming Lin, Natalia Gimelshein, Luca Antiga, Alban Desmaison, Andreas Köpf, Edward Yang, Zach DeVito, Martin Raison, Alykhan Tejani, Sasank Chilamkurthy, Benoit Steiner, Lu Fang, Junjie Bai, and Soumith Chintala. Pytorch: An imperative style, high-performance deep learning library. In *Advances in Neural Information Processing Systems (NeurIPS)*, 2019. 7, 12
- [36] Jie Qin, Jiemin Fang, Qian Zhang, Wenyu Liu, Xingang Wang, and Xinggang Wang. Resizemix: Mixing data with preserved object information and true labels. *arXiv preprint arXiv:2012.11101*, 2020. 8, 12, 15
- [37] Shaoqing Ren, Kaiming He, Ross Girshick, and Jian Sun. Faster r-cnn: Towards real-time object detection with region proposal networks. *arXiv preprint arXiv:1506.01497*, 2015. 8, 13
- [38] Joshua David Robinson, Ching-Yao Chuang, Suvrit Sra, and Stefanie Jegelka. Contrastive learning with hard negative samples. In *International Conference on Learning Representations*, 2021. 5
- [39] Olga Russakovsky, Jia Deng, Hao Su, Jonathan Krause, Sanjeev Satheesh, Sean Ma, Zhiheng Huang, Andrej Karpathy, Aditya Khosla, Michael Bernstein, et al. Imagenet large scale visual recognition challenge. *International journal of computer vision*, pages 211–252, 2015. 6
- [40] Ramprasaath R. Selvaraju, Michael Cogswell, Abhishek Das, Ramakrishna Vedantam, Devi Parikh, and Dhruv Batra. Gradcam: Visual explanations from deep networks via gradient-based localization. *arXiv preprint arXiv:1610.02391*, 2019. 1, 13
- [41] Zhiqiang Shen, Zechun Liu, Zhuang Liu, Marios Savvides, Trevor Darrell, and Eric Xing. Un-mix: Rethinking image mixtures for unsupervised visual representation learning. In *Proceedings of the Conference on Computer Vision and Pattern Recognition (CVPR)*, 2021. 1, 7, 8, 15
- [42] Yonglong Tian, Dilip Krishnan, and Phillip Isola. Contrastive multiview coding. In *Proceedings of the European Conference on Computer Vision (ECCV)*, 2020. 3, 13
- [43] Yonglong Tian, Chen Sun, Ben Poole, Dilip Krishnan, Cordelia Schmid, and Phillip Isola. What makes for good views for contrastive learning? In *Advances in Neural Information Processing Systems (NeurIPS)*, 2020. 4, 13
- [44] Naftali Tishby, Fernando C Pereira, and William Bialek. The information bottleneck method. *ArXiv*, physics/0004057, 2000. 2
- [45] Yao-Hung Hubert Tsai, Yue Wu, Ruslan Salakhutdinov, and Louis-Philippe Morency. Self-supervised learning from a multi-view perspective. In *International Conference on Learning Representations (ICLR)*, 2021. 4
- [46] AFM Uddin, Mst Monira, Wheemyung Shin, TaeChoong Chung, Sung-Ho Bae, et al. Saliencycymix: A saliency guided data augmentation strategy for better regularization. *arXiv preprint arXiv:2006.01791*, 2020. 1, 8, 12, 15
- [47] Aaron van den Oord, Yazhe Li, and Oriol Vinyals. Representation learning with contrastive predictive coding. *arXiv preprint arXiv:1807.03748*, 2019. 2, 3
- [48] Vikas Verma, Alex Lamb, Christopher Beckham, Amir Najafi, Ioannis Mitliagkas, David Lopez-Paz, and Yoshua Bengio. Manifold mixup: Better representations by interpolating hidden states. In *International Conference on Machine Learning*, pages 6438–6447. PMLR, 2019. 8, 12, 15
- [49] Catherine Wah, Steve Branson, Peter Welinder, Pietro Perona, and Serge Belongie. The caltech-ucsd birds-200-2011 dataset. California Institute of Technology, 2011. 6, 12
- [50] X. Wang, R. Girshick, A. Gupta, and K. He. Non-local neural networks. In *2018 IEEE/CVF Conference on Computer Vision and Pattern Recognition*, pages 7794–7803, 2018. 5
- [51] Eric Wong, Leslie Rice, and J Zico Kolter. Fast is better than free: Revisiting adversarial training. 2020. 8
- [52] Yuxin Wu, Alexander Kirillov, Francisco Massa, Wan-Yen Lo, and Ross Girshick. Detectron2. <https://github.com/facebookresearch/detectron2>, 2019. 8
- [53] Saining Xie, Ross Girshick, Piotr Dollár, Zhuowen Tu, and Kaiming He. Aggregated residual transformations for deep neural networks. In *Proceedings of the IEEE conference on computer vision and pattern recognition*, pages 1492–1500, 2017. 6
- [54] Sangdoo Yun, Dongyoon Han, Seong Joon Oh, Sanghyuk Chun, Junsuk Choe, and Youngjoon Yoo. Cutmix: Regularization strategy to train strong classifiers with localizable features. In *Proceedings of the IEEE/CVF International Conference on Computer Vision*, pages 6023–6032, 2019. 1, 3, 4, 8, 12, 15
- [55] Xiaohang Zhan, Jiahao Xie, Ziwei Liu, Yew Soon Ong, and Chen Change Loy. Online deep clustering for unsupervised representation learning. In *Proceedings of the Conference on Computer Vision and Pattern Recognition (CVPR)*, 2020. 4, 12, 13

- [56] Hongyi Zhang, Moustapha Cisse, Yann N Dauphin, and David Lopez-Paz. mixup: Beyond empirical risk minimization. *arXiv preprint arXiv:1710.09412*, 2017. [1](#), [3](#), [4](#), [8](#), [12](#), [15](#)
- [57] Jianchao Zhu, Liangliang Shi, Junchi Yan, and Hongyuan Zha. Automix: Mixup networks for sample interpolation via cooperative barycenter learning. In *European Conference on Computer Vision*. Springer, 2020. [1](#)

## A. Appendix

We first provide implementation details for supervised (SL) and self-supervised learning (SSL) tasks in A.1, and detailed experiment settings for Sec. 3 in A.2. Then, we visualize mixed samples in A.3. Moreover, we provide more experiment results in A.4 and detailed related work in A.5.

### A.1. Implementation Details

#### A.1.1 Basic Settings

**Reproduction details.** We use MMclassification<sup>1</sup> and OpenSelfSup<sup>2</sup> in PyTorch [35] as our code-base for both supervised image classification and contrastive learning (CL) tasks. Except results marked by † and ‡, we reproduce most experiment results of compared methods, including Mixup [56], CutMix [54], ManifoldMix [48], SaliencyMix [46], FMix [16], and ResizeMix [36].

**Dataset information.** We briefly introduce image datasets used in Sec. 4: (1) CIFAR-100 [28] contains 50k training images and 10K test images of 100 classes. (2) ImageNet-1k (IN-1k) [29] contains 1.28 million training images and 50k validation images of 1000 classes. (3) Tiny-ImageNet (Tiny) [8] is a rescaled version of ImageNet-1k, which has 100k training images and 10k validation images of 200 classes. (4) STL-10 [10] benchmark is designed for semi- or unsupervised learning, which consists of 5k labeled training images for 10 classes and 100k unlabelled training images, and a test set of 8k images. (5) CUB-200-2011 (CUB) [49] contains over 11.8k images from 200 wild bird species for fine-grained classification. (6) FGVC-Aircraft (Aircraft) [34] contains 10k images of 100 classes of aircrafts. (7) iNaturalist2017 (iNat2017) [22] is a large-scale fine-grained classification benchmark consisting of 579.2k images for training and 96k images for validation from over 5k different wild species. (8) PASCAL VOC [13] is a classical objection detection and segmentation dataset containing 16.5k images for 20 classes. (9) COCO [31] is an objection detection and segmentation benchmark containing 118k scenic images with many objects for 80 classes.

#### A.1.2 Supervised Image Classification

**Implementation of SAMix.** We provide detailed implementation of SAMix in SL tasks. As shown in Figure 3 (left), we adopt the momentum pipeline [15, 32] to optimize  $\mathcal{L}_{\theta, \omega}$  for mixup classification and  $\mathcal{L}_{\phi}$  for mixup generation in Eq. 5 in an end-to-end manner:

$$\theta_q^t, \omega_q^t \leftarrow \underset{\theta, \omega}{\operatorname{argmin}} \mathcal{L}_{\theta_q^{t-1}, \omega_q^{t-1}}, \quad (10)$$

$$\phi^t \leftarrow \underset{\phi}{\operatorname{argmin}} \mathcal{L}_{\theta_k^t, \omega_k^t} + \mathcal{L}_{\phi^{t-1}}, \quad (11)$$

where  $t$  is the iteration step,  $\theta_q, \omega_q$  and  $\theta_k, \omega_k$  denote the parameters of online and momentum networks, respectively. The parameters in the momentum networks are an exponential moving average of the online networks with a momentum decay coefficient  $m$ , taking  $\theta_k$  as an example,

$$\theta_k^t \leftarrow m\theta_k^{t-1} + (1 - m)\theta_q^t. \quad (12)$$

The SAMix training process is summarized as four steps: (1) using the momentum encoder to generate the feature maps  $Z^l$  for Mixer  $\mathcal{M}_{\phi}$ ; (2) generating  $X_{mix}^q$  and  $X_{mix}^k$  by Mixer for the online networks and Mixer; (3) training the online networks by Eq. 10 and the Mixer by Eq. 11 separately; (4) updating the momentum networks by Eq. 12.

**Hyper-parameter settings.** As for hyper-parameters of SAMix, we follow the basic setting in AutoMix for both SL and SSL tasks: SAMix adopts  $\alpha = 2$ , the feature layer  $l = 3$ , the bilinear upsampling, and the weight  $\beta = 0.1$  which linearly decays to 0. We use  $\eta = 0.5$  for small-scale datasets (CIFAR-100, Tiny, CUB and Aircraft) and  $\eta = 0.1$  for large-scale datasets (IN-1k and iNat2017). As for other methods, PuzzleMix [26], Co-Mixup [25], and AugMix [21] are reproduced by their official implementations with  $\alpha = 1, 2, 1$  for all datasets. We provide dataset-specific hyper-parameter settings for our reproduced mixup methods: For CIFAR-100, Mixup and ResizeMix use  $\alpha = 1$ , and CutMix, FMix and SaliencyMix use  $\alpha = 0.2$ , and ManifoldMix uses  $\alpha = 2$ . For Tiny, IN-1k, and iNat2017, ManifoldMix uses  $\alpha = 0.2$ , and the rest methods adopt  $\alpha = 1$  for median and large backbones (e.g., ResNet-50). Specially, all these methods use  $\alpha = 0.2$  (only) for ResNet-18. For small-scale fine-grained datasets (CUB-200 and Aircraft), SaliencyMix and FMix use  $\alpha = 0.2$ , and ManifoldMix uses  $\alpha = 0.5$ , while the rest use  $\alpha = 1$ .

#### A.1.3 Contrastive Learning

**Implementation of SAMix-C and SAMix-I.** As for SSL tasks, we adopt the cross-view objective,  $\ell^{NCE}(z_i^{\tau_q}, z_i^{\tau_k}) + \ell^{NCE}(z_m)$ , where  $z_i = z_i^{\tau_k}$  and  $z_j = z_j^{\tau_k}$ , for instance-level mixup classification in all methods (except for † and ‡ marked methods). We provide two variants, SAMix-C and SAMix-I, which use different learning objectives of mixup classification. Based on network structures (an encoder  $f_{\theta}$  and a projector  $g_{\omega}$ ) in MoCo.V2 [6], SAMix-C is similar to SAMix in SL tasks, using a parametric cluster classification head  $g_{\psi}^C$  for online clustering [3, 55]. Notice that  $g_{\psi}^C$  is used for  $\mathcal{L}_{\phi}^{cls}$ . It takes feature vectors from the momentum encoder as the input (optimized by Eq. 11) and does not affect the mixup classification objective for online networks. Meanwhile, SAMix-I uses the instance-level classification loss for both  $\mathcal{L}_{\theta, \omega}$  and  $\mathcal{L}_{\phi}^{cls}$ . Notice that we use  $\eta$ -balanced mixup loss  $\mathcal{L}_{\phi}^{cls}$  for both SAMix-C and SAMix-I with  $\eta = 0.5$  and the objective  $\mathcal{L}_{\phi}$  for Mixer is the same as in SL tasks.

<sup>1</sup><https://github.com/open-mmlab/MMclassification>

<sup>2</sup><https://github.com/open-mmlab/OpenSelfSup>



**Hyper-parameter settings.** Except for SwAV [4], all CL-based methods use MoCo.V2 pre-training settings, which uses ResNet [20] as the encoder  $f_\theta$  with two-layer MLP projector  $g_\omega$  and is optimized by SGD optimizer and Cosine scheduler with the initial learning rate of 0.03 and the batch size of 256. The length of the momentum dictionary is 65536 for IN-1k and 16384 for STL-10 and Tiny. The data augmentation strategy is based on IN-1k in MoCo.v2 as following: Geometric augmentation is RandomResizedCrop with the scale in  $[0.2, 1.0]$  and RandomHorizontalFlip. Color augmentation is ColorJitter with {brightness, contrast, saturation, hue} strength of  $\{0.4, 0.4, 0.4, 0.1\}$  with a probability of 0.8, and RandomGrayscale with a probability of 0.2. Blurring augmentation is using square Gaussian kernel of size  $23 \times 23$  with a std uniformly sampled in  $[0.1, 2.0]$ . We use  $224 \times 224$  resolutions for IN-1k and  $96 \times 96$  resolutions for STL-10 and Tiny.

**Evaluation protocols.** We evaluate the SSL representation with a linear classification protocol proposed in MoCo [17], which trains a linear classifier on top of the frozen representation on the training set. The linear classifier is trained 100 epochs by a SGD optimizer with the SGD momentum of 0.9 and the weight decay of 0. We set the initial learning rate of 30 for IN-1k as MoCo, and 0.1 for STL-10 and Tiny. The learning rate decays by 0.1 at epoch 60 and 80. Moreover, we use object detection task to evaluate transfer learning abilities following MoCo, which use the 4-th layer feature maps of ResNet (ResNet-C4) to train Faster R-CNN [37] with 24k iterations on the *trainval07+12* set (16.5k images) and Mask R-CNN [18] with  $2 \times$  schedule on the *train2017* set (118k images).

## A.2. Empirical Experimental Settings

### A.2.1 Analysis of Instance-level Mixup

In Sec. 3.1, we propose the cross-view training pipeline for mixup classification (shown in Figure 3 (a)) and discuss inter- and intra-class proprieties of instance-level mixup. We verify them by two experiments: Firstly, as shown in Figure 3 (b), we compare using the same-view or cross-view pipelines combined with using  $\ell^{NCE}(z_i^{\tau_q}, z_i^{\tau_k}) + \ell^{NCE}(z_m)$  or only using  $\ell^{NCE}(z_m)$  with ResNet-18 pre-training 400-epoch on Tiny. Then, as shown in Figure 3 (c), we adopt inter-cluster and intra-cluster mixup from {Mixup, CutMix} with  $\alpha \in \{0.2, 1, 2, 4\}$  to verify that instance-level mixup should treat inter- and intra-class mixup differently. Empirically, mixed samples provided by Mixup preserve global information of both source samples (smoother) while samples generated by CutMix preserve local patches (more discriminative). And we introduce pseudo labels (PL) to indicate different clusters by clustering method ODC [55] with the class (cluster) number  $C$ . Based on experiment results, we can conclude that inter-class mixup requires *discriminative*

mixed samples with *strong* intensity while the intra-class needs *smooth* samples with *low* intensity. Moreover, we provide two cluster-based instance-level mixup methods in Table 3 and 4 (denoting by \*): (a) Inter-Intra\*. We use CutMix with  $\alpha \geq 2$  as inter-cluster mixup and Mixup with  $\alpha = 0.2$  as intra-cluster mixup. (b) PuzzleMix\*. We introduce saliency-based mixup methods to SSL tasks by introducing PL and a parametric cluster classifier  $g_\psi^C$  after the encoder. This classifier  $g_\psi^C$  and encoder  $f_\theta$  are optimized alternatively like SAMix mentioned in A.1.2. Based on grad-CAM [40] calculated from the classifier, PuzzleMix can be adopted on SSL tasks.

### A.2.2 Analysis of Mixup Generation Objectives

In Sec. 3.2, we design experiments to analyze various losses for mixup generation in Figure 5 (left) and the proposed  $\eta$ -balanced loss in Figure 5 (right) for both SL and SSL tasks with ResNet-18 on STL-10 and Tiny. Basically, we assume both STL-10 and Tiny datasets have 200 classes on their 100k images. Since STL-10 does not provide ground truth labels (L) for 100k unlabeled data, we introduce PL generated by a supervised pertained classifier on Tiny as the "ground truth" for its 100k training set. Notice that L denotes ground truth labels and PL denotes pseudo labels generated by ODC [55] with  $C = 200$ .

As for the SL task, we use the labeled training set for mixup classification (100k on Tiny v.s. 5k on STL-10). Notice that SL results are worse than using SSL settings on STL-10, since the SL task only trains a randomly initialized classifier on 5k labeled data. Because the infoNCE and BCE loss require cross-view augmentation (or they will produce trivial solutions), we adopt MoCo.V2 augmentation settings for these two losses when performing the SL task. Compared to CE (L), we corrupt the global term in CE as CE (PL) or directly remove them as pBCE (L) to show that pBCE is vital to optimizing mixed samples. Similarly, we show that the global term is used as the global constrain by comparing BCE (UL) with infoNCE (UL), infoNCE (PL) and infoNCE (L). As for the SSL task, we use the same training setting as A.1.3, and verify the conclusions drawn from the SL task. We can conclude that (a) the local term optimizes mixup generation directly, corresponding to the smoothness property, (b) the global term serves as the global constraint corresponding to the discriminative property. Moreover, we verified that using the  $\eta$ -balanced loss as  $\mathcal{L}_\phi^{cls}$  yields best performance on SL and SSL tasks. Notice that we use  $\eta = 0.5$  on small-scale datasets and  $\eta = 0.1$  on large-scale datasets for SL tasks, and use  $\eta = 0.5$  for all SSL tasks.

### A.2.3 Analysis of Mutual Information for Mixup

Since mutual information (MI) as usually adopted to analyze contrastive-based augmentations [42, 43], we estimate MI

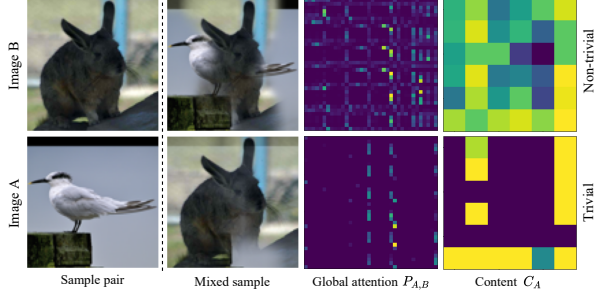


Figure 9. Visualization of the trivial solution of Mixer in SAMix-I on STL-10. The upper row shows non-trivial results produced by Mixer with the non-linear content sub-module  $C_{NCL}$  while the lower row shows the trivial solution (such as constant  $s_i$ ) using the linear  $C$ .

between  $x_m$  of various methods and  $x_i$  by MINE [1] with 100k images in  $64 \times 64$  resolutions on Tiny. We sample  $\lambda =$  from 0 to 1 with the step of 0.125 and plot results in Figure 8 (d). Here we see that SAMix-C and SAMix-I with more MI when  $\lambda \approx 0.5$  perform better.

### A.3. Visualization of SAMix

#### A.3.1 Mixing Attention and Content in Mixer

In Sec. 3.3, we discuss the trivial solutions of Mixer, which are usually occurred in SSL tasks. Given the sample pair  $(x_i, x_j)$  and  $\lambda = 0.5$ , we visualize the content  $C_i$  and  $P_{i,j}$  to compare the trivial and non-trivial results in the SSL task on STL-10, as shown in Figure 9. As we can see, both  $C_i$  and  $P_{i,j}$  from the trivial solution has extremely large or small scale values while  $C_i$  generated by  $C_{NCL}$  containing more balanced values. Since the attention weight  $P_{i,j}$  is normalized by softmax, we hypothesize that  $C_i$  more likely causes trivial solutions. To verify our hypothesis, we freeze  $W_P$  in the original MB and compare the original linear content projection  $W_z$  with the non-linear content modeling. The results confirm that the non-linear module can prevent large-scale values on  $C_i$  and eliminate the trivial solutions.

#### A.3.2 Effects of Mixup Generation Loss

In addition to Sec. 3.4, we further provide visualization of mixed samples using the infoNCE (Eq. 4), BCE (Eq. 7), and  $\eta$ -balanced infoNCE loss (Eq. 8) for Mixer. As shown in Figure 10, we find that mixed samples using infoNCE mixup

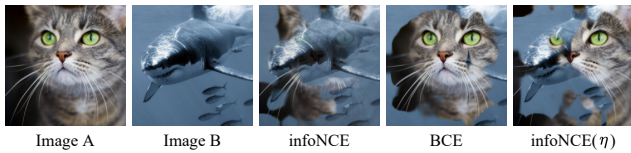


Figure 10. Visualization of loss effect. Both infoNCE and BCE loss have different emphases: infoNCE shows the similar effect of supervised fine-grained classification, focusing on fragmented and essential features, while BCE focuses on object completeness.

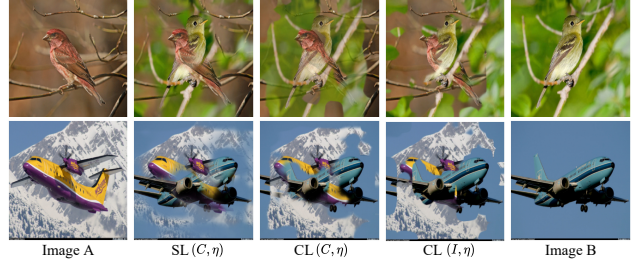


Figure 11. Visualization of SAMix in various scenarios on CUB and Aircraft. Given images A and B, the middle three mixed samples are generated by SAMix with  $\lambda = 0.5$  trained in the fine-grained SL task and the SSL tasks (SAMix-C and SAMix-I).

loss prefer instance-specific and fine-grained features. On the contrary, mixed samples of the BCE loss seem only to consider discrimination between two corresponding neighborhood systems. It is more inclined to maintain the continuity of the whole object relative to infoNCE. Thus, combining both the characteristics, the  $\eta$ -balanced infoNCE loss yields mixed samples that retain both instance-specific features and global discrimination.

#### A.3.3 Visualization of Mixed Samples in SAMix

**SAMix in various scenarios.** In addition to Sec. 3.4, we visualize the mixed samples of SAMix in various scenarios to show the relationship between mixed samples and class (cluster) information. Since IN-1k contains some samples in CUB and Aircraft, we choose the overlapped samples to visualize SAMix trained for the fine-grained SL task (CUB and Aircraft) and SSL tasks (SAMix-I and SAMix-C). As shown in Figure 11, mixed samples reflect the granularity of class information adopted in mixup training. Specifically, we find that mixed samples using infoNCE mixup loss (Eq. 4) is more closely to the fine-grained SL because they both have many fine-grained centroids.

**Comparison with PuzzleMix in SL tasks.** To highlight the accurate mixup relationship modeling in SAMix compared to PuzzleMix (standing for saliency-based methods), we visualize results of mixed samples from these two methods in the supervised case in Figure 12. There are three main difference: (a) bilinear upsampling strategy in SAMix makes the mixed samples more smooth in local patches. (b) adaptive  $\lambda$  encoding and mixing attention enhance the correspondence between mixed samples and  $\lambda$  value. (c)  $\eta$ -balanced mixup loss enables SAMix to balance global discriminative and fine-grained features.

#### Comparison of SAMix-I and SAMix-C in SSL tasks.

As shown in Figure 13, we provide more mixed samples of SAMix-I and SAMix-C in the SSL tasks to show that introducing class information by PL can help Mixer generate mixed samples that retain both the fine-grained features (instance discrimination) and whole targets.

#### A.4. More Experiments

We provide more results of SL tasks on CIFAR-100 and IN-1k. Firstly, we train SAMix and compared methods with 400, 800, 1200 epochs on CIFAR-100 based on ResNet-18 (R-18) and ResNeXt-50 (32x4d) (RX-50), as shown in Table 9. SAMix steadily outperforms previous methods regardless of the training time setting. Notice that † denotes reproduced results by official source code and other results are reproduced by us. And \* denotes unpublished work on arxiv. Then we provide comparing results under 100-epoch training protocol on IN-1k with various network architectures, as shown in Table 10. SAMix outperforms previous methods and improves the vanilla by 0.85%, 1.11%, 1.18%, 1.69%, and 1.73% based on R-18, R-34, R-50, R-101, and RX-101 on IN-1k.

Method	R-18			RX-50		
	400ep	800ep	1200ep	400ep	800ep	1200ep
Vanilla	77.73	78.04	78.55	80.24	81.09	81.32
MixUp	79.34	79.12	79.24	82.54	82.10	81.77
CutMix	79.58	78.17	78.29	78.52	78.32	77.17
ManifoldMix	80.18	80.35	80.21	82.56	82.88	83.28
SaliencyMix	79.64	79.12	77.66	78.63	78.77	77.51
FMix*	79.91	79.69	79.50	78.99	79.02	78.24
PuzzleMix†	80.22	80.43	80.64	82.84	82.57	82.85
ResizeMix*	79.19	80.01	79.23	79.78	80.35	79.73
AutoMix*	81.78	82.04	81.95	83.32	83.64	83.80
<b>SAMix</b>	<b>81.97</b>	<b>82.30</b>	<b>82.41</b>	<b>83.85</b>	<b>84.11</b>	<b>84.23</b>
Gain	+0.19	+0.26	+0.46	+0.53	+0.57	+0.43

Table 9. Top-1 accuracy (%) of image classification on CIFAR-100.

Method	R-18	R-34	R-50	R-101	RX-101
Vanilla	70.04	73.85	76.93	78.18	78.71
MixUp	69.98	74.07	77.12	78.97	79.56
CutMix	68.95	73.14	77.07	78.96	79.59
ManifoldMix	69.98	74.11	76.91	79.02	79.68
SaliencyMix	69.12	73.18	77.15	79.01	79.65
FMix*	68.37	73.04	77.20	79.09	79.62
AugMix†	-	-	77.23	-	-
PuzzleMix†	70.12	74.26	77.54	79.34	79.94
Co-Mixup†	-	-	77.60	-	-
SuperMix†	-	-	77.61	-	-
ResizeMix*	69.50	73.88	77.57	79.27	79.87
AutoMix*	70.47	74.50	77.76	79.68	80.23
<b>SAMix</b>	<b>70.85</b>	<b>74.96</b>	<b>78.11</b>	<b>79.87</b>	<b>80.44</b>
Gain	+0.38	+0.34	+0.35	+0.19	+0.21

Table 10. Top-1 accuracy (%) on ImageNet-1k training 100-epoch based on various network architectures.

#### A.5. Detailed related work

**Contrastive Learning.** CL amplifies the potential of SSL by achieving significant improvements on classification [4, 5, 7, 17], which maximizes similarities of positive pairs while minimizes similarities of negative pairs. To provide a global

view of CL, MoCo [17] proposes a memory-based framework with a large number of negative samples and model differentiation using the exponential moving average. SimCLR [5] demonstrates a simple memory-free approach with a large batch size and strong data augmentations that is also competitive in performance to memory-based methods. Unlike other CL approaches, BYOL [15] does not require negative pairs or a large batch size for the proposed pretext task, which tries to estimate latent representations from the same instance.

**Mixup.** MixUp [56], convex interpolations of any two samples and their unique one-hot labels, were presented as the first mixing-based data augmentation approach for regularising the training of networks. ManifoldMix [48] and PatchUp [14] expand it to the hidden space. CutMix [54] suggests a mixing strategy based on the patch of the image, *i.e.*, randomly replacing a local rectangular section in images. Based on CutMix, ResizeMix [36] inserts a whole image into a local rectangular area of another image after scaling down. FMix [16] converts the image to Fourier space (spectrum domain) to create binary masks. To generate more semantic virtual samples, offline optimization algorithms are introduced for the saliency regions. SaliencyMix [46] obtains the saliency using a universal saliency detector. With optimization transportation, PuzzleMix [26] and Co-Mixup [25] present more precise methods for finding appropriate mixup masks based on saliency statistics. SuperMix [11] combines mixup with knowledge distillation, which learns a pixel-wise sample mixing policy via a teacher-student framework to distill class knowledge. Differing from previous methods, AutoMix [32] can learn the mixup generation by a sub-network end-to-end which generated mixed samples via feature maps and the mixing ratio.

**Mixup for contrastive learning.** A complementary method for better instance-level representation learning is to use mixup on CL [23, 41]. When used in collaboration with CE loss, Mixup and its several variants provide highly efficient data augmentation for SL by establishing a relationship between samples. Without a ground-truth label, the most of approaches are limited to linear mixup methods. For example, Un-mix [41] attempts to use MixUp in the input space for self-supervised learning, whereas the developers of MoChi [23] propose mixing the negative sample in the embedding space to increase the number of hard negatives but at the expense of classification accuracy. i-Mix [30] and BSIM [9] demonstrated how to regularize contrastive learning by mixing instances in the input or latent spaces. We introduce automatic mixup for SSL tasks, which adaptively learns the instance relationship based on inter- and intra-cluster properties online.



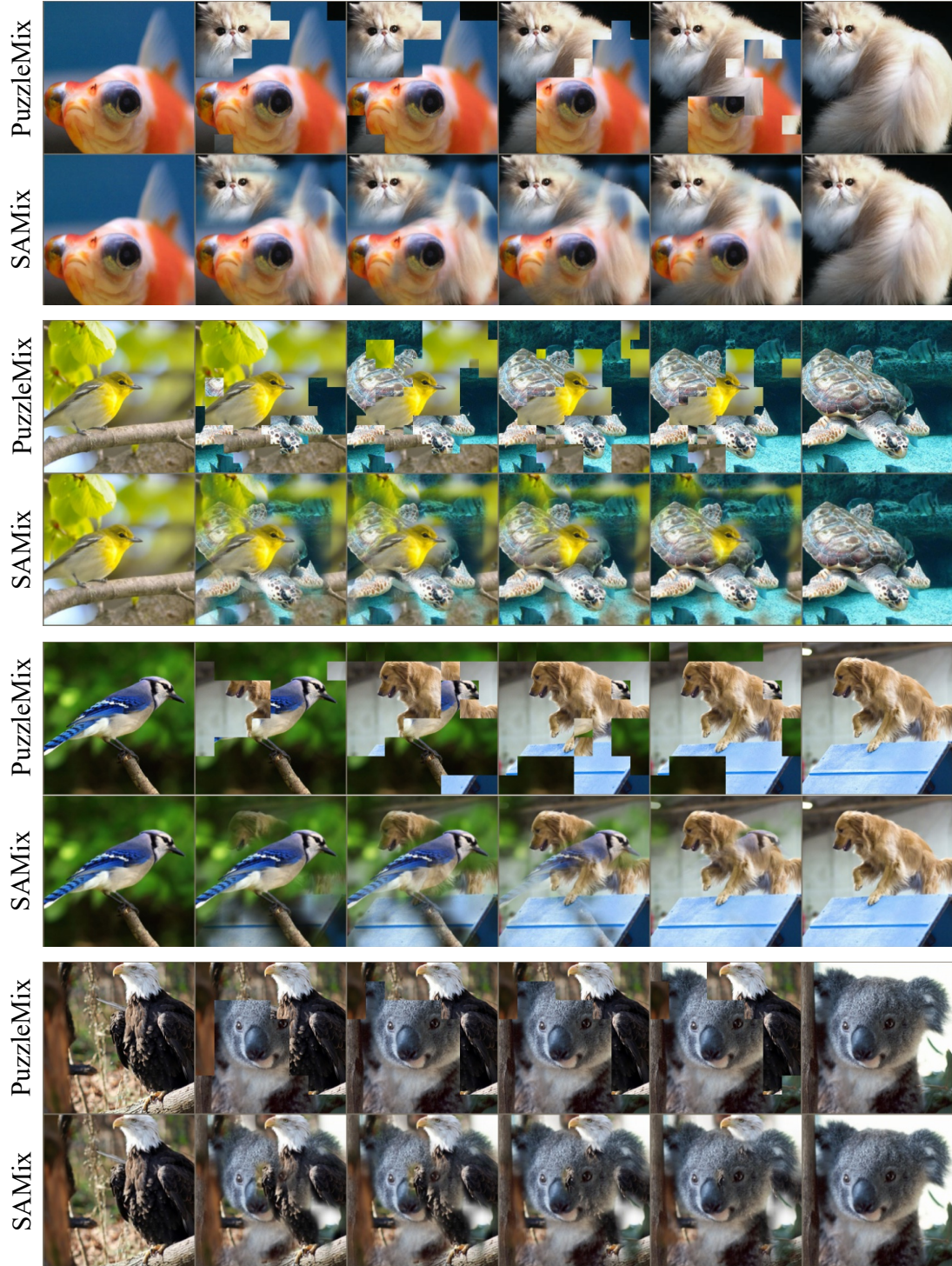


Figure 12. Visualization of PuzzleMix v.s. SAMix for SL tasks on IN-1k. In each four rows, the upper and lower two rows represent mixed samples generated by PuzzleMix and SAMix, respectively.  $\lambda$  value changes from left ( $\lambda = 0$ ) to right ( $\lambda = 1$ ) by an equal step.



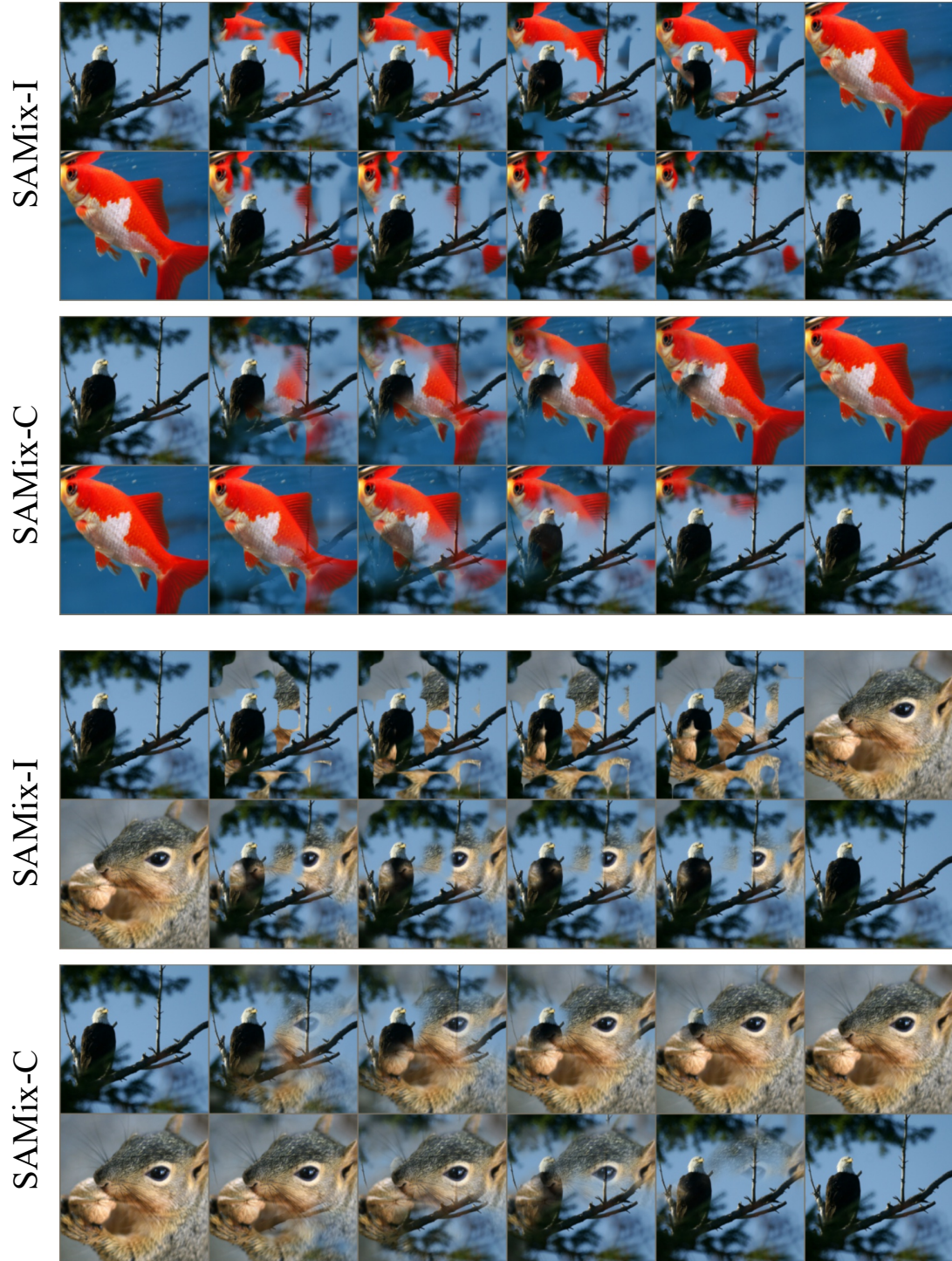


Figure 13. Visualization of SAMix-I v.s. SAMix-C for SSL tasks on IN-1k. In each four rows, the upper and lower two rows represent mixed samples generated by SAMix-I and SAMix-C, respectively.  $\lambda$  value changes from left ( $\lambda = 0$ ) to right ( $\lambda = 1$ ) by an equal step.